Principal-ray delay across a finite solar-lens pupil

A conditional comparison with a geometric smearing estimate

16 November 2026
Technical note; preprint, not peer reviewed
Version 1.0.0

Abstract

A 2020 solar-lens communications preprint assigns a characteristic geometric delay of approximately five nanoseconds to a one-metre receiver aperture. We examine a natural, explicitly defined reconstruction: the range of principal stationary-ray group arrivals across one fixed receiver pupil, illuminated by a finite coherent transmitter. In a scalar Fresnel model with an absorbing solar disk and a Schwarzschild phase screen, a one-metre pupil at 650 astronomical units has a span enclosed by 25.867–26.046 femtoseconds. This is the standard point-lens differential-delay calculation, supplemented by a bound for the finite transmitter at one parsec; no new lensing law is proposed. The preprint does not specify exact endpoint coordinates or derive its asserted path excess, so the comparison is conditional on the reconstructed geometry rather than a refutation of every possible smearing statistic. The quoted nanosecond scale does not describe this principal-ray span. The coherent received pulse, available temporal modes, communications capacity and the actual solar environment are not calculated.

1 Question and source interpretation

Hippke's 2020 preprint, version 1 [1], describes simultaneous transmission, one physical receiver aperture, and rays labelled by impact parameters b and $b + w$, identifying w with the receiver diameter D. Its Eq. (14) states

$$\Delta t_{\text{quoted}} = \sqrt{2}D/c, \tag{1}$$

rounded there to 5 ns for $D = 1$ m, and describes this scale as independent of focal distance. A local gravitational clock-dilation estimate is considered separately. The source uses this temporal-smearing premise to motivate restrictions on receiver size and temporal encoding.

The text and schematic figures do not specify the exact compared endpoint coordinates or derive the asserted $\sqrt{2}w$ path excess. They do not define Eq. (1) as an RMS width, percentile, or rigorous lower bound. We therefore distinguish its assertion from our reconstruction:

Source assertion	Reconstruction tested here
One receiver aperture, labelled impact rays $b, b + w$, with $w = D$	A centered disk of radius $a = D/2$ in one fixed receiver plane; stationary paths determine the impact coordinates
Simultaneous emission; unspecified exact path endpoints	One specified coherent source field with a common phase reference, propagated to that plane
Characteristic geometric excess $\sqrt{2}D$	Supremum minus infimum of principal stationary-ray group arrivals over that disk

This is a physically natural reconstruction, not an authenticated derivation of the source's unspecified endpoints. Our conclusion concerns applying Eq. (1) to this reconstruction, not every possible timing observable intended by the source.

2 Model, coordinates and observable

Place the source plane at $z = -z_{\rm s}$, lens plane at $z = 0$, and receiver plane at $z = z_{\rm r}$, with transverse coordinates $\boldsymbol{u}$, $\boldsymbol{b}$ and $\boldsymbol{\rho}$. The receiver disk is $|\boldsymbol{\rho}| \le a$. The source amplitude is

$$u_{\rm tx} = C_{\rm tx} e^{-|\boldsymbol{u}|^2/w_0^2} \mathbf{1}_{|\boldsymbol{u}|\le d}, \qquad C_{\rm tx}^{-2} = \frac{\pi w_0^2}{2}(1 - e^{-2d^2/w_0^2}), \tag{2}$$

so $\int |u_{\rm tx}|^2 d^2u = 1$. Its phase is flat and its spatial shape is frequency independent. We take $d = 1\,\mathrm{m}$, $w_0 = 0.5\,\mathrm{m}$, $z_{\rm s} = 1\,\mathrm{pc}$, $z_{\rm r} = 650\,\mathrm{AU}$, $a = 0.5\,\mathrm{m}$ and carrier wavelength $\lambda_0 = 1\,\mu\mathrm{m}$.

The defining scalar propagation operator is $P_{z_{\rm r}} Q P_{z_{\rm s}}$, with

$$(P_L f)(\boldsymbol{x}) = \frac{k e^{ikL}}{2\pi i L} \int e^{ik|\boldsymbol{x}-\boldsymbol{y}|^2/(2L)} f(\boldsymbol{y}) d^2y, \tag{3}$$

$$Q(\boldsymbol{b}) = \mathbf{1}_{r \ge R_\odot} e^{-2ikr_{\rm s}\ln(r/R_\odot)}, \quad r = |\boldsymbol{b}|, \quad k = \omega/c, \quad r_{\rm s} = 2GM/c^2. \tag{4}$$

The disk is perfectly absorbing in this scalar model. P_L is unitary in transverse L^2 and composes as free Fresnel propagation; Q is a contraction. Removed norm is not renormalized. These are normalization controls, not collection-efficiency calculations or a full-Maxwell reduction.

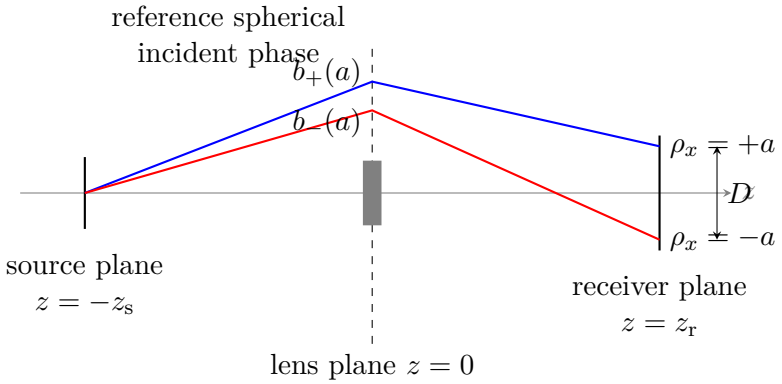


Figure 1: Coordinate schematic, not to scale. The drawn paths are extremal reference paths in a meridional section, with positive impact coordinates and opposite receiver edges. Reflection supplies their partners. For each nonzero receiver radius there are two principal branches; on axis there is a ring. The actual coherent source is a disk, not the point illustrating the reference spherical wavefront. Equations, not drawing angles or lengths, define the geometry.

Define the principal branches as phase-stationary paths continuously connected to the usual focal ring and lying in $R_\odot \le r \le 2R_\odot$. Each branch is assigned the partial ω derivative of its total stationary phase at the carrier, with one common reference removed. The observable is the supremum minus infimum of these values over the whole receiver disk and both branches. It is not the derivative of the argument of the complete coherent field.

3 Reference result: standard point-lens delay

Factor the incident spherical phase and temporarily omit the residual finite-source phase. For $Z = (1/z_{\rm s} + 1/z_{\rm r})^{-1}$ the reduced optical length is

$$L_0 = \frac{r^2}{2Z} - \frac{\boldsymbol{b}\cdot\boldsymbol{\rho}}{z_{\rm r}} + \frac{\rho^2}{2z_{\rm r}} - 2r_{\rm s}\ln(r/R_\odot). \tag{5}$$

The geometric and gravitational signs follow directly from the operator. Put $b_E = \sqrt{2r_{\rm s}Z}$, $x = Z\rho/z_{\rm r}$ and $S = \sqrt{x^2 + 4b_E^2}$. The two radial magnitudes are

$$b_+(\rho) = (S + x)/2, \qquad b_-(\rho) = (S - x)/2, \tag{6}$$

with vectors aligned and opposite to $\boldsymbol{\rho}$, respectively. Reference arrivals $\tau_\pm = L_0/c$ satisfy

$$\frac{d\tau_+}{d\rho} = \frac{\rho - b_+}{cz_{\rm r}} < 0, \qquad \frac{d\tau_-}{d\rho} = \frac{\rho + b_-}{cz_{\rm r}} > 0. \tag{7}$$

They agree on axis. The full reference span occurs at the pupil boundary:

$$D_0 = \tau_-(a) - \tau_+(a) = \frac{1}{c}\left[\frac{aS(a)}{2z_{\rm r}} + 2r_{\rm s}\ln\frac{b_+(a)}{b_-(a)}\right]. \tag{8}$$

For $a \ll b_E$, $D_0 \sim 2b_E a/(cz_{\rm r})$. This is the standard point-lens two-image differential-delay expression: with $y = Za/(z_{\rm r}b_E)$,

$$D_0 = \frac{2r_{\rm s}}{c}\left[\frac{y\sqrt{y^2+4}}{2} + \ln\frac{\sqrt{y^2+4}+y}{\sqrt{y^2+4}-y}\right]. \tag{9}$$

The logarithmic monopole potential and finite-telescope point-spread treatment are established solar-lens ingredients; see, for example, Loutsenko [2]. That reference is cited for these ingredients, not as evidence that it states the finite-pupil arrival span considered here. Neither the differential-delay identity nor its small-pupil limit is a new lensing law. The application at issue is the particular numerical premise in Eq. (1).

4 Control of the coherent finite transmitter

After extracting the incident spherical phase and common factors, the exact residual source field is

$$C(k, r) = \mathbb{E}_w[e^{ik|\boldsymbol{u}|^2/(2z_{\rm s})}\cos(kru_x/z_{\rm s})]. \tag{10}$$

Here $\mathbb{E}_w$ uses positive normalized *amplitude* weight $e^{-|\boldsymbol{u}|^2/w_0^2}$ on the source disk. Pairing u_x and $-u_x$ yields the cosine. Contributions combine coherently before taking a phase.

Set $A = d^2/(2z_{\rm s})$, $T = d/z_{\rm s}$, $B = 2R_\odot$ and

$$m = 1 - \tfrac{1}{2}[(kA)^2 + (kBT)^2]. \tag{11}$$

At the carrier $kBT < 0.284$, $kA < 1.02 \times 10^{-10}$ and $m > 0.959$. Using $\cos v \geq 1 - v^2/2$ in this positive-cosine range gives $\mathrm{Re}\, C \geq m$, so the continuous phase $\phi = \arg C$ has no singularities in the principal annulus. Compact-integral differentiation and $|\sin v| \leq |v|$ give

$$|\phi_r| \leq P = \frac{k^2BT^2}{m}, \qquad |\phi_{rr}| \leq Q = \frac{(kT)^2}{m} + P^2, \tag{12}$$

$$|\phi_k| \leq H = \frac{A + kB^2T^2}{m}. \tag{13}$$

For $\rho > 0$, axisymmetry places stationary points along or opposite to $\boldsymbol{\rho}$. The radial equations are

$$\frac{r}{Z} - \frac{2r_{\rm s}}{r} - s\frac{\rho}{z_{\rm r}} + \frac{\phi_r}{k} = 0, \qquad s = +1, -1. \tag{14}$$

Their derivatives are positive because $Q/k < 1/Z$. Each root lies within $\delta = ZP/k$ of its reference root: shifting that root by $\pm\delta$ changes the unperturbed radial function by at least $\pm P/k$, enclosing the perturbation. Both brackets lie strictly between $R_\odot$ and B uniformly for

$0 \le \rho \le a$. This proves uniqueness of each principal radial branch, including the degenerate on-axis ring. The bounds remain valid while replacing ϕ by $t\phi$, $0 \le t \le 1$. This does not classify distant source sidelobes or edge-diffraction terms.

The total phase is $kL_0 + \phi$. Stationarity removes the branch-position derivative, giving group arrival $(L_0 + \phi_k)/c$. Since L_0 is stationary at the reference root and $\partial_r^2 L_0 \le J = 1/Z + 2r_\mathrm{s}/R_\odot^2$, each arrival differs from its reference by at most

$$e = \frac{J\delta^2/2 + H}{c}, \qquad |D_\mathrm{actual} - D_0| \le 2e. \tag{15}$$

This uniform bound remains valid if the true extrema shift from the pupil boundary.

5 Enclosure and interpretation

The constants are $c = 299792458\,\mathrm{m\,s^{-1}}$, $GM = 1.32712440018 \times 10^{20}\,\mathrm{m^3\,s^{-2}}$, $R_\odot = 6.957 \times 10^8\,\mathrm{m}$, $\mathrm{AU} = 149597870700\,\mathrm{m}$, and $\mathrm{pc} = (648000/\pi)\,\mathrm{AU}$, treated as exact model inputs.

Rational interval arithmetic gives $D_0 = 25.95624141134\,\mathrm{fs}$ to the displayed precision, $\delta < 0.000928\,\mathrm{m}$ and $2e < 0.088794\,\mathrm{fs}$. A conservative enclosure is

$$\boxed{25.867\,\mathrm{fs} < D_\mathrm{actual} < 26.046\,\mathrm{fs}.} \tag{16}$$

Equation (1) gives $4.717308673499\,\mathrm{ns}$; our upper endpoint is less than 5.522×10^{-6} of that scale. The spherical reference differs from its plane-incident limit, $25.997107049882\,\mathrm{fs}$ at the same receiver distance, by only $0.040866\,\mathrm{fs}$.

The spherical-reference impact annulus width is $b_+(a) - b_-(a) = Za/z_\mathrm{r} \simeq 0.49843\,\mathrm{m}$, rather than $D = 1\,\mathrm{m}$. The exact finite-source roots have the bounded perturbations established above; their annulus width differs by at most 2δ. A factor-of-two annulus convention cannot explain the much larger delay discrepancy. The geometric contribution to Eq. (8) is about $13\,\mathrm{fs}$ and the gravitational contribution also about $13\,\mathrm{fs}$: they add for these endpoints. The outer-impact path in Fig. 1 arrives earlier in this reference geometry. Including Shapiro delay does not cancel this entire geometric spread.

The quoted scale cannot supply the principal-ray delay premise for the reconstructed fixed-pupil geometry. Since the source does not show its exact endpoint construction, this is a conditional clarification, not a proof against every possible intended meaning of "smearing." We make no claim of literature-wide priority for the formula or its application.

6 Limitations and conclusion

The sub-femtosecond enclosure is a within-model error bound. It excludes physical-constant uncertainties and corrections from higher gravitational orders, plasma, solar multipoles, spin, pointing and detector response. It is not an accuracy statement for the actual Sun.

A derivative of an individual stationary phase is not the derivative of the argument of the coherent sum. Branch interference, the on-axis caustic, source sidelobes and absorbing-edge diffraction can affect the full waveform. No approximation error for that waveform has been bounded here. Thus the result is not a pulse duration, arrival-time probability distribution, causal-front calculation, temporal-mode count or capacity improvement. Those require additional analysis.

Standard point-lens optics, with controlled finite coherent illumination, gives a roughly $26\,\mathrm{fs}$ principal-ray span for this pupil. It challenges using $4.7\,\mathrm{ns}$ as that span under the stated reconstruction. This limited source-specific comparison is the purpose of the note; the general optics is established.

Reproducibility

The supplement contains two distinct rational checks. One encloses Eq. (8) using $v - v^3/6 \leq \operatorname{asinh} v \leq v$ and rationally verified square-root brackets. The other integrates the envelope identity $D_0'(\rho) = \sqrt{(Z\rho/z_\mathrm{r})^2 + 4b_E^2}/(cz_\mathrm{r})$ between its endpoint bounds. Both include Eq. (15), nonzero-phase and branch-domain controls. Exact rational endpoints, not rounded diagnostic decimals, are authoritative. Python's standard library suffices; instructions and previously calculated outputs are supplied. Neither script simulates a received pulse.

References

[1] M. Hippke, *Interstellar communication network. II. Deep space nodes with gravitational lensing*, arXiv:2009.01866v1 (2020), arxiv.org/abs/2009.01866v1. Comparison concerns this preprint version, particularly its receiver-size/temporal-smearing discussion and Eq. (14), not an unexamined revised journal text.

[2] I. Loutsenko, *On the role of caustics in solar gravitational lens imaging*, Progress of Theoretical and Experimental Physics **2018**, 123A02 (2018), doi:10.1093/ptep/pty119.